Correlative analysis of vertebral trabecular bone microarchitecture and mechanical properties: a combined ultra-high field (7 Tesla) MRI and biomechanical investigation

Daphnée Guenoun, Alexandre Fouré, Martine Pithioux, Sandrine Guis, Thomas Lecorroller, Jean Pierre Mattei, Vanessa Pauly, Maxime Guye, Monique Bernard, Patrick Chabrand, et al.

HAL Id: hal-01593111

https://hal.science/hal-01593111

Submitted on 15 Nov 2017

Correlative analysis of vertebral trabecular bone microarchitecture and mechanical properties: a combined ultra-high field (7 Tesla) MRI and biomechanical investigation

DaphneGuenoun, MD (1,2); Alexandre Fouré, PhD (3); Martine Pithioux, PhD (2); Sandrine Guis, MD, PhD (4); Thomas Le Corroller, MD, PhD, APHM (1,2); Jean-Pierre Mattei, MD (4) ; Vanessa Pauly, PhD (5,6) ; Maxime Guye, MD, PhD (3); Monique Bernard, PhD (3); Patrick Chabrand, PhD (2) ; Pierre Champsaur, MD, PhD (1,2); David Bendahan, PhD (3)

(1) APHM, Sainte-Marguerite Hospital, Institute for Locomotion, Department of Radiology, 13009, Marseille, France
(2) Aix Marseille Univ, CNRS, ISM, InstMovementSci, Marseille, France
(3) Aix Marseille Univ, CNRS, CRMBM UMR 7339, 13385, Marseille, France
(4) Rheumatologydepartment 1, Aix-Marseille Université, CNRS, CRMBM UMR 7339, AP-HM, Marseille, France
(5) Aix Marseille Univ, Unité de recherche EA3279, Santé Publique et Maladies Chroniques: Qualité de vie concepts, usages et limites, déterminants, 13005, Marseille, France
(6) APHM, Service de Santé Publique et d'Information Médicale, Hôpital de la Conception, Marseille, France

Corresponding author:

Daphne GUENOUN, *MD*
APHM, Sainte-Marguerite Hospital, Institute for Locomotion
Department of Radiology, 13009, Marseille, France
Aix Marseille Univ, CNRS, ISM, InstMovementSci, 13009, Marseille, France
Daphne.guenoun@ap-hm.fr
Tel: 0033(0)649319326   Fax: 0033(0)491744821

Abstract

Study Design: High resolution imaging and biomechanical investigation ofex-vivo vertebrae

Objective: To assess bone microarchitecture of cadavericvertebrae using ultra-high field (UHF) 7 Tesla magnetic resonance imaging (MRI) and todetermine whether the corresponding microarchitecture parameters were related to BMD andbone strength assessed by dual energy X-ray absorptiometry (DXA) and mechanicalcompression tests.

Summary of Background Data: Limitations of DXA for theassessment of bone fragility and osteoporosis have been recognized and criteriaof microarchitecture alteration have been included in the definition of osteoporosis. Although vertebral fracture is the most commonosteoporotic fracture, no study has assessed directly vertebral trabecular bone. microarchitecture.

Methods: BMD of twenty four vertebrae (L2, L3, L4) from eight cadavers were investigatedusing DXA. The bone volume fraction (BVF), trabecular thickness (Tb.Th), and trabecularspacing (Tb.Sp) of each vertebra was quantified using UHF MRI. Measurements wereperformed by two operators in order to characterize the inter-rater reliability. The whole set ofspecimens underwent mechanical compression tests to failure and the corresponding failurestress was calculated.

Results: The inter-rater reliability for bone microarchitecture parameters was good with intraclass correlation coefficients ranging from 0.82 to 0.94. Failure load and stress weresignificantly correlated with BVF, Tb.Sp and BMD ($p < 0.05$). Tb.Th was only correlatedwith the failure stress ($p < 0.05$). Multiple regression analysis demonstrated that thecombination of BVF and BMD improved the prediction of the failure stress from an adjusted $R^2 = 0.384$ for BMD alone to an adjusted $R^2 = 0.414$.

Conclusions: We demonstrated for the first time that the vertebral bone microarchitectureassessed with UHF MRI was significantly correlated with biomechanical parameters. Ourdata suggest that the multimodal assessment of BMD and trabecular bone microarchitecturewith UHF MRI provides

additional information on the risk of vertebral bone fracture andmight be of interest for the future

investigation of selected osteoporotic patients.

Introduction

Osteoporosis is an age-related progressive skeletal disease characterized by a low bone mass and microarchitectural alterations resulting in an increased bone fragility and susceptibility to fracture [1]. Vertebral fractures are the most common type of osteoporotic fracture and are associated with a decreased quality of life [2] and a substantial morbidity[3]. Given that BMD measured by dual-energy X-ray absorptiometry (DXA) and fracture risk were found to be highly correlated, DXA has become the standard diagnostic test for osteoporosis [4,5]. Accordingly, osteoporosis is defined as a BMD T-score higher than 2.5 standard deviations (SD) below the peak bone mass [5]. However, it has been shown that vertebral fractures can occur in women with BMD values below 2.5 SD [6] so that limitations of DXA for the assessment of bone fragility and osteoporosis diagnosis have been recognized [7] and criteria of microarchitecture alteration have been included in the definition of osteoporosis [1].

Bone microarchitecture can be assessed in 3D using *in vitro* micro-CT (μCT) [8,9] or *in vivo* using high resolution quantitative computed tomography (HR-QCT). Using HR-QCT, it has been found in post-menopausal women that vertebral and non-vertebral fractures were partly associated to architectural alterations of the trabecular bone at the distal radius and tibia [10]. However, HR-QCT cannot be used in clinical routine due to image blurring and large X-ray exposure [11]. In that context, techniques with broad availability, such as X-ray or bone densitometry can appear as attractive [12-14]. However, these projectional methods transform a 3D structure into a 2D image, and remain indirect. In contrast, magnetic resonance imaging (MRI) is a non-ionizing radiation imaging technique and can be used to assess trabecular bone structure. MRI has already been used *in vivo* at peripheral sites such as the distal radius [15], the calcaneus [16], the distal tibia [17,18] and the femoral neck [19]. On the basis of measurements of trabecular architecture, the corresponding studies reported altered bone microarchitecture in patients with fragility fractures. High-resolution MRI of trabecular bone may

represent a powerful technique to gain insights into trabecular bone microarchitectural alterations in osteoporosis. In addition, ultra high-field (UHF) MRI might be of additional interest given the potential gain regarding signal to noise ratio and images spatial resolution as compared to conventional MRI using magnetic fields from 1.5 to 3T [20]. In several previous studies, vertebral fracture risk has been assessed on the basis of microarchitecture measurement using MRI of the wrist [21] or distal femur [18]. Besides, quantification of vertebral bone marrow fat content has been assessed to indirectly determine potential alteration of cancellous bone using 3T MR spectroscopy [22]. To the best of our knowledge, no study has ever compared microarchitecture of vertebral trabecular bone using MRI and biomechanical parameters. In addition, although vertebral fracture is the most common osteoporotic fracture, no study has assessed directly vertebral trabecular bone microarchitecture.

The aim of the present study was to directly investigate bone microarchitecture of cadaveric vertebrae using UHF MRI and to determine the relationship with failure load and stress assessed during mechanical compression and BMD obtained with DXA.

Materials and methods

Vertebral specimens

Twenty-four lumbar vertebrae (L2, L3, L4) from spines of 8 human donors, 6 women and 2 men (age: 82 (9) yrs) were obtained at the Anatomy Department within 10 days after death, in accordance with institutional safety and ethics regulations. Donor consent for research purposes was obtained prior to death. No information was available on the cause of death or previous diseases. All specimens were carefully cleaned of muscle tissue, intervertebral disc and ligaments. The specimens were stored at −20°C. All specimens were thawed at room temperature for 6 hours before testing. Thus, only one defrosting cycle was required. After defrosting, all vertebrae were first investigated using UHF MRI then, scanned using computer tomography, scanned using DXA in order to determine the BMD, and compressed in order to determine the failure load.

Magnetic resonance imaging

Each specimen was placed in a rectangular plastic box (Huenersdorff GmbH, Ludwigsburg, Germany; length: 200 mm, width: 100 mm, height: 94 mm) filled with one liter of saline solution (i.e., sodium chloride, 9 g.L^{-1}).

Vertebrae were investigated using an UHF whole body MRI scanner (MAGNETOM 7T, Siemens Medical System, Erlangen, Germany). A 28-channel ^{1}H knee coil was used for trabecular bone imaging. After scout images acquisitions in the three orthogonal plans, an interactive localized B$_0$ shimming was performed using the second-order shimming procedure provided by the manufacturer. High-resolution gradient recalled-echo images of each vertebra were acquired in both the axial and sagittal planes with the following parameters: field of view = 140 × 140 mm²; matrix = 832 × 832; time repetition = 20 ms; time echo = 6 ms; flip angle = 15°; number of repetitions = 3 and no gap between slices. Slice thickness of 0.4 mm and 0.5 mm were used for acquisition in the axial and sagittal plans respectively. The corresponding acquisition time was 34 min 11 s and 51 min 16 s for axial and sagittal explorations.

Using an open-source digital measurement software (ImageJ, NIH, Bethesda, MD, USA), Dicom images were initially cropped in order to keep the slices of interest. Thereafter, images were thresholded to obtain a set of binary images. The threshold was manually determined using the same procedure for the whole set of images. A first set of slice was saved and a second set of slice was additionally cropped to obtain a 15 × 15 × 15 mm^3 volume of interest at the center of the vertebra (Figure 1A-D).

Apparent bone volume fraction (BVF) corresponding to bone volume scaled to the total volume ratio (BV/TV), trabecular thickness (Tb.Th) and trabecular spacing (Tb.Sp) were assessed with BoneJ[23], a plugin of ImageJ, dedicated to the assessment of the cancellous bone microarchitecture. Analyses were performed for the two sets of images (i.e., whole vertebra and center of the vertebra) by two

independent operators, a 6 year experience skeletal radiologist and an physician doctor specialized in MRI.

The inter-rater reliability of microarchitecture characterization was assessed with an intraclass correlation coefficient (ICC) for each microarchitecture variable [24]. The average coefficient of variation between rater was presented as CV.

CT measurements

Each vertebra was scanned using GE Light Speed VCT 64 (FOV small, thickness 0.625 x 0.625 mm, mA 365, kV 120) in order to check the presence of tissue fibrosis or vertebral lesion. 3D reconstructions were done to measure the surface of the superior plate of the vertebral body. This measure was used to calculate the failure stress.

DXA measurements

The specimens were positioned similarly to *in vivo* conditions in a vessel filled with tap water up to 15 cm in height to simulate soft tissue. DXA measurements were performed with a Lunar iDXA Scanner (GE/Lunar; GE Medical Systems, Milwaukee, WI, USA). BMD was measured in each vertebral body for each specimen.

Mechanical testing

An imprint of the end plates of each vertebra was made using a common epoxy resin [25]. The resin enabled vertebrae to be set in the vertical axis of the compression device. The vertebrae were then placed between plates on a materials testing machine as previously described [14] (Instron 5566, Instron, Canton, MA, USA). Each specimen was loaded to failure at a 5 mm/min velocity [26]. The failure load in Newton (N) and the failure stress in Megapascal (MPa) were recorded.

Statistics

To assess the correlations among parameters, the Spearman rho correlation coefficient (ρ) was computed. The level of significance was set at $p < 0.05$. Results are reported as mean (SD).

Then a multiple regression analysis was performed and the coefficient of determination adjusted R² was reported.

Statistical analysis was made using SPSS V20.

Results

The CT analysis showed the presence of tissue fibrosis from unknown origin inside three vertebrae (from the same cadaver) which were excluded from the final analysis. An additional vertebra was excluded for technical issues during the mechanical tests. The statistical analysis was then performed on 20 vertebrae.

Bone microarchitecture indices and mechanical tests values

The mean BMD values were 0.86 (0.2) g/cm². During the mechanical test, the mean failure load was 2823 (1203) N. The mean failure stress was 2.54 (1.22) MPa.

In the whole vertebra, the mean BVF in the axial and sagittal planes were 0.55 (0.12) and 0.52 (0.12), respectively. The averaged Tb.Th value was 0.49 (0.08) mm in the axial and 0.49 (0.14) mm in the sagittal plane. The mean Tb.Sp value was 0.44 (0.08) mm in the axial plane 0.46 (0.09) mm in the sagittal plane.

Measures computed in the whole vertebra and the cropped volume of interest were significantly correlated ($p < 0.01$) (Figure 2AB). On that basis, only results obtained in the whole vertebra were reported.

The ICC for the microarchitecture measurements performed in the axial plane were 0.92 (CV = 7%) for BVF, 0.87 (CV=6.6%) for Tb.Th and 0.82 (CV=5.2%) for Tb.Sp. In the sagittal plane, the corresponding ICC were 0.82 (CV= 10.7%) for BVF, 0.88 (CV=10.1%) for Tb.Th and 0.94 (CV=4.3%) for Tb.Sp.

Measures computed in the axial and sagittal planes were significantly correlated ($p < 0.01$) (Table 1).

Correlation between the microarchitecture indices

BVF was strongly correlated with Tb.Th ($\rho = 0.89$ in the axial plane and $\rho = 0.88$ in the sagittal plane) and Tb.Sp ($\rho = 0.57$ in the axial plane and $\rho = -0.84$ in the sagittal plane) ($p < 0.01$) (Figure 3AB). Tb.Th and Tb.Sp were correlated in the sagittal plane ($p < 0.05$) but not in the axial plane (Table 1).

Correlation between mechanical stress indices, BMD and bone microarchitecture

BMD was significantly correlated with the failure load ($\rho = 0.63$; $p = 0.003$) and failure stress ($\rho = 0.66$; $p = 0.002$) (Figure 4A). The bone volume fraction was also correlated with the failure load ($\rho = 0.52$; $p = 0.02$) and the failure stress ($\rho = 0.63$; $p = 0.003$) (Figure 4B). In the sagittal plane, Tb.Th was also correlated with the failure stress $\rho = 0.50$ ($p = 0.02$). Tb.Sp was significantly correlated with the failure load ($p < 0.05$) and stress ($p < 0.01$) in both axial and sagittal planes (Table 2).

Accordingly, in both axial ($\rho = 0.60$; $p = 0.004$) and sagittal planes ($\rho = 0.46$; $p = 0.03$) BMD was linearly linked to the bone volume fraction (Figure 4C). BMD was also significantly correlated with the Tb.Th in the axial plane ($\rho = 0.47$; $p = 0.03$) and Tb Sp in the sagittal plane ($\rho = 0.51$; $p = 0.01$).

Multiple regression analysis demonstrated that combining BVF and BMD improved of 7.8 % the failure stress prediction from an adjusted $R^2=0.384$ for BMD alone to an adjusted $R^2 =0.414$ for the combination of BMD and BVF.

Combining Th.Th and BMD or Tb.Sp and BMD did not improved the failure stress prediction with respectively an adjusted $R^2 =0.374$ and adjusted $R^2 =0.381$.

Discussion

In the present study, we intended to evaluate vertebral bone microarchitecture using UHF-MRI and to characterize the potential relationships with BMD, the commonly used index for the diagnosis of osteoporosis on the one hand and quantitative indices related to mechanical tests on the other hand.

As previously described [14, 27], BMD was strongly correlated with both quantitative mechanical variables i.e. failure load and stress. Interestingly, the bone volume fraction and trabecular space were also linked to the mechanical variables while the trabecular thickness was significantly related to the

failure stress. The combination of BMD and BVF improved the statistical power of the correlation with the mechanical variables thereby suggesting that the combined measurements of BMD and bone microarchitecture might be of interest for our understanding of bone quality and the early diagnosis of osteoporosis regarding vertebral fractures.

Although BMD is largely considered as the standard diagnostic variable of osteoporosis [5], the limited sensitivity of BMD has been suggested [28;29]. In a large cohort of patients, Jager et al. [29] reported a prevalence of vertebral fracture of 14% in patients with normal BMD.

Although BMD can predict vertebral bone strength to some extent, it has been suggested that other bone quality factors such as macroarchitecture, microarchitecture, mineralization, size and quality of the crystal, as well as rate of bone turnover can be considered as significant contributors [30]. Among these variables, microarchitecture has been suggested as one of the most relevant contributors being part of the definition of osteoporosis [31,32].

A study conducted *ex vivo* in lumbar vertebrae assessed vertebral microarchitecture using high-resolution peripheral quantitative computed tomography (HR-pQCT) and mechanical compression. They founded that BMD alone explained up to 44% of the variability in vertebral mechanical behavior, bone volume fraction up to 53%, and trabecular architecture up to 66% [33].

Overall, the issue of whether the bone microarchitecture analysis has the potential to assess bone quality, complementary to and independent of BMD measurements, has become a crucial research topic.

A few publications have described MRI of trabecular bone at UHF [20, 34, 35]; and all these studies suggest strong potential for UHF to improve imaging of trabecular bone *via* increases in spatial resolution or reduced scan time. Because vertebral bone microarchitecture has not been studied at UHF MRI, we evaluated the feasibility of this imaging modality on *ex-vivo* vertebrae.

The volume of interest was the whole vertebral body excluding cortical bone and the posterior arch and a cropped region in the center of the vertebra (15 x 15 x 15 mm3). The methodology was in accordance

with what reported by Hulme *et al*. [9]who used μCT and who concluded that vertebral fracture strength could not be explained through analysis of one specific region. In our study, we founded a perfect matching between the measures made on the whole vertebra and the cropped volume of interest.

In agreement with previous studies, we reported a strong relationship between BMD and the biomechanical parameters[14]. Interestingly, BMD was also strongly correlated with the bone volume fraction which is in agreement with the study of Field *et al*. [36] who studied trabecular microarchitecture of human thoracic vertebral bodies using μCT and finite element models. In the later study, a good correlation between bone mineral content (BMC) measured with DXA (BMC= BMD x W (width at the scanned line)) and BV/TV (= BVF) ($r = 0.58$; $p < 0.01$) was found. However, in contrast to the present results, no significant correlation between BMC and Tb.Th or Tb.Sp was established. This discrepancy can be explained by the choice of the T9 vertebral body which is a smaller vertebra as compared to the lumbar vertebra we analyzed in our study. Furthermore, only the center of the vertebra with a region of interest of about 15x15x10 mm was analyzed whereas we studied the whole trabecular bone of the vertebra. Finally this difference could be inherent to the technique of bone imaging.

In our study, BVF seemed to be the best bone microarchitecture parameter with significant correlation with failure load and stress. BVF is related to porosity and can be considered as a surrogate of volumetric bone density rather than a strict measure of bone microarchitecture [36]. These results are supportive of previous MRI studies of bone microarchitecture, which were carried out in the distal radius, ankle, distal femur and wrist [15, 16, 18]. At 1.5T, Majumbar *et al*. [15] reported a lower BVF in the distal radius of subjects with fragility fractures (mean BVF = 0.23) as compared to controls (mean BVF = 0.29)while Link *et al*. [16]showed a similar result in the calcaneal bone. Chang *et al*. [18] founded that BVF of the distal femur at 7T MRI can help to detect women with fragility fractures who do not differ by BMD [18].They reported that BVF measured on distal femoral metaphysic was about 0.31 in the control group whereas it was about 0.03 in fracture cases. There was no difference in

trabecular thickness between the two groups. Finally, Greenspan *et al.* [21] found at 1.5T that BVF measured in the wrist, was lower in men with vertebral fracture as compared to healthy controls.

In our study, Tb.Sp was correlated to biomechanical tests. Link *et al.* [16] also observed that Tb.Sp measured on the calcaneus at 1.5T discriminated osteoporotic subjects without osteoporotic hip fractures, with a mean Tb.Sp of 1.38 mm, from patients with osteoporotic hip fractures, with a mean Tb.Sp of 1.85 mm.

In the present study, strong correlations between BVF and other microarchitectural variables were found (Table 1; Figure 3) suggesting a potential overlap between these variables for the assessment of bone quality.

Although correlations were found to be higher with measurements in the axial plane as compared to those performed in the sagittal plane, we cannot provide clear explanation at this stage. However, this result prompts us to advise the axial plane for the assessment of vertebral bone microarchitecture using UHF MRI. Previous MRI studies performed on the distal femur [18], the calcaneus and the distal radius [15] have also reported measurements in the axial plane.

A few issues might be raised regarding the methodological aspects of the present study. Our results have been obtained from a small number of specimens although this number is similar to what has been reported in the literature [14, 36]. One might be concerned by the initial freezing before the measurements, the removal of soft tissue and the potential degradation of the samples. In that respect, the ranges of BMD and failure load values we reported were similar to those previously reported from *ex vivo* studies[37].

We acknowledge that UHF MRI is not widely available and that the resolution we obtained was still lower than what one can obtain with HR-QCT. However, HR-QCT cannot be used in clinical routine due to image blurring and large X-ray exposure.

Although we selected the most currently used microarchitecture parameters i.e. BVF, Tb.Sp and Tb.Th, additional parameters might be of interest.

Overall, we have demonstrated in the present study that UHF 7T MRI could be considered as a promising technique for future bone microarchitecture analyses *in vivo*. The MRI-derived bone microarchitecture parameters were correlated with BMD measurements on the one hand and the bone strength on the other hand. To the best of our knowledge, this study is the first to analyze vertebral bone microarchitecture parameters using UHF 7 Tesla MRI. These data obtained *ex vivo* should now be extended to the clinical context with the assessment of selected patients with different levels of fracture risks who were not detected by the DXA.

References

1. Consensus development conference: diagnosis, prophylaxis, and treatment of osteoporosis. Am J Med. 1993;94(6):646–50.

2. Lips P, van Schoor NM. Quality of life in patients with osteoporosis. Osteoporos Int J Establ Result Coop Eur Found Osteoporos Natl Osteoporos Found USA. 2005;16(5):447–55.

3. Kendler DL, Bauer DC, Davison KS, et al. Vertebral Fractures: Clinical Importance and Management. Am J Med. 2016 ;129(2):221.e1-10.

4. Kanis JA. Diagnosis of osteoporosis and assessment of fracture risk. Lancet Lond Engl. 2002; 359(9321):1929–36.

5. Marshall D, Johnell O, Wedel H. Meta-analysis of how well measures of bone mineral density predict occurrence of osteoporotic fractures. BMJ. 1996; 312(7041):1254–9.

6. Schuit SCE, van der Klift M, Weel AE a. M, et al. Fracture incidence and association with bone mineral density in elderly men and women: the Rotterdam Study. Bone 2004;34(1):195–202.

7. Mccreadie BR, Goldstein SA. Biomechanics of Fracture: Is Bone Mineral Density Sufficient to Assess Risk? J Bone Miner Res. 2000; 15(12):2305–8.

8. Feldkamp LA, Goldstein SA, Parfitt AM, et al. The direct examination of three-dimensional bone architecture in vitro by computed tomography. J Bone Miner Res Off J Am Soc Bone Miner Res. 1989; 4(1):3–11.

9. Hulme PA, Boyd SK, Ferguson SJ. Regional variation in vertebral bone morphology and its contribution to vertebral fracture strength. Bone 2007; 41(6):946–57.

10. Sornay-Rendu E, Boutroy S, Munoz F, Delmas PD. Alterations of cortical and trabecular architecture are associated with fractures in postmenopausal women, partially independent of decreased BMD measured by DXA: the OFELY study. J Bone Miner Res Off J Am Soc Bone Miner Res. 2007; 22(3):425–33.

11. Lespessailles E, Chappard C, Bonnet N, et al. Imaging techniques for evaluating bone microarchitecture. Jt Bone Spine Rev Rhum. 2006; 73(3):254–61.

12. Harvey NC, Glüer CC, Binkley N, et al. Trabecular bone score (TBS) as a new complementary approach for osteoporosis evaluation in clinical practice. Bone 2015; 78:216–24.

13. Eriksson SA, Isberg BO, Lindgren JU. Prediction of vertebral strength by dual photon absorptiometry and quantitative computed tomography. Calcif Tissue Int. 1989; 44(4):243–50.

14. Guenoun D, Le Corroller T, Acid S, et al. Radiographical texture analysis improves the prediction of vertebral fracture: an ex vivo biomechanical study. Spine 2013; 38(21):E1320-1326.

15. Majumdar S, Link TM, Augat P, et al. Trabecular bone architecture in the distal radius using magnetic resonance imaging in subjects with fractures of the proximal femur. Magnetic Resonance Science Center and Osteoporosis and Arthritis Research Group. Osteoporos Int J Establ Result Coop Eur Found Osteoporos Natl Osteoporos Found USA. 1999; 10(3):231–9.

16. Link TM, Majumdar S, Augat P, et al. In vivo high resolution MRI of the calcaneus: differences in trabecular structure in osteoporosis patients. J Bone Miner Res Off J Am Soc Bone Miner Res. 1998;13(7):1175–82.

17. Wehrli FW, Saha PK, Gomberg BR, et al. Role of magnetic resonance for assessing structure and function of trabecular bone. Top Magn Reson Imaging TMRI. 2002; 13(5):335–55.

18. Chang G, Honig S, Liu Y, et al. 7 Tesla MRI of bone microarchitecture discriminates between women without and with fragility fractures who do not differ by bone mineral density. J Bone Miner Metab. 2015; 33(3):285–93.

19. Gomberg BR, Saha PK, Wehrli FW. Method for cortical bone structural analysis from magnetic resonance images. Acad Radiol. 2005;12(10):1320–32.

20. Chang G, Wang L, Liang G, et al. Reproducibility of subregional trabecular bone micro-architectural measures derived from 7-Tesla magnetic resonance images. Magma N Y N. 2011; 24(3):121–5.

21. Greenspan SL, Wagner J, Nelson JB, et al. Vertebral Fractures and Trabecular Microstructure in Men with Prostate Cancer on Androgen Deprivation Therapy. J Bone Miner Res Off J Am Soc Bone Miner Res. 2013; 28(2):325–32.

22. Li X, Kuo D, Schafer AL, et al. Quantification of Vertebral Bone Marrow Fat Content using 3 Tesla MR spectroscopy: Reproducibility, Vertebral Variation and Applications in Osteoporosis. J Magn Reson Imaging JMRI. 2011; 33(4):974–9.

23. Doube M, Kłosowski MM, et al. BoneJ: free and extensible bone image analysis in ImageJ. Bone. 2010; 47(6):1076–9.

24. Shrout PE, Fleiss JL. Intraclass correlations: uses in assessing rater reliability. Psychol Bull. 1979; 86(2):420–8.

25. Belkoff SM, Mathis JM, Jasper LE, et al. The biomechanics of vertebroplasty. The effect of cement volume on mechanical behavior. Spine 2001; 26(14):1537–41.

26. Tohmeh AG, Mathis JM, Fenton DC, et al. Biomechanical efficacy of unipedicular versus bipedicular vertebroplasty for the management of osteoporotic compression fractures. Spine 1999; 24(17):1772–6.

27. Seo SH, Lee J, Park IH. Efficacy of Dual Energy X-ray Absorptiometry for Evaluation of Biomechanical Properties: Bone Mineral Density and Actual Bone Strength. J Bone Metab 2014; 21(3):205–12.

28. Ferrar L, Jiang G, Adams J, et al. Identification of vertebral fractures: an update. Osteoporos Int J Establ Result Coop Eur Found Osteoporos Natl Osteoporos Found USA. 2005; 16(7):717–28.

29. Jager PL, Jonkman S, Koolhaas W, et al. Combined vertebral fracture assessment and bone mineral density measurement: a new standard in the diagnosis of osteoporosis in academic populations. Osteoporos Int J Establ Result Coop Eur Found Osteoporos Natl Osteoporos Found USA. 2011; 22(4):1059–68.

30. Seeman E, Delmas PD. Bone quality--the material and structural basis of bone strength and fragility. N Engl J Med. 2006; 354(21):2250–61.

31. Briggs AM, Greig AM, Wark JD. The vertebral fracture cascade in osteoporosis: a review of aetiopathogenesis. Osteoporos Int J Establ Result Coop Eur Found Osteoporos Natl Osteoporos Found USA. 2007; 18(5):575–84.

32. Yeni YN, Zinno MJ, Yerramshetty JS, et al. Variability of trabecular microstructure is age-, gender-, race- and anatomic site-dependent and affects stiffness and stress distribution properties of human vertebral cancellous bone. Bone 2011;49(4):886–94.

33. Wegrzyn J, Roux J-P, Arlot ME, et al. Role of trabecular microarchitecture and its heterogeneity parameters in the mechanical behavior of ex vivo human L3 vertebrae. J Bone Miner Res Off J Am Soc Bone Miner Res. 2010; 25(11):2324–31.

34. Krug R, Carballido-Gamio J, Banerjee S, Stahl R, Carvajal L, Xu D, et al. In vivo bone and cartilage MRI using fully-balanced steady-state free-precession at 7 tesla. Magn Reson Med. 2007; 58(6):1294–8.

35. Magland JF, Rajapakse CS, Wright AC, Acciavatti R, Wehrli FW. 3D fast spin echo with out-of-slab cancellation: a technique for high-resolution structural imaging of trabecular bone at 7 Tesla. Magn Reson Med. 2010; 63(3):719–27.

36. Fields AJ, Eswaran SK, Jekir MG, et al. Role of Trabecular Microarchitecture in Whole-Vertebral Body Biomechanical Behavior. J Bone Miner Res. 2009; 24(9):1523–30.

37. Lim T-H, Brebach GT, Renner SM, et al. Biomechanical evaluation of an injectable calcium phosphate cement for vertebroplasty. Spine (Phila Pa 1976) 2002;27(12):1297–302.

Figures legend:

Figure 1: A: axial high resolution 7 T MR image of the vertebra. B: Threshold image of the vertebra in the axial plane. C: sagittal high resolution 7 T MR image of the vertebra. D: Threshold image of the vertebra in the sagittal plane. We analyzed the whole area of trabecular bone (yellow volume of interest) and a cropped volume of interest in the center of the vertebra (red rectangle).
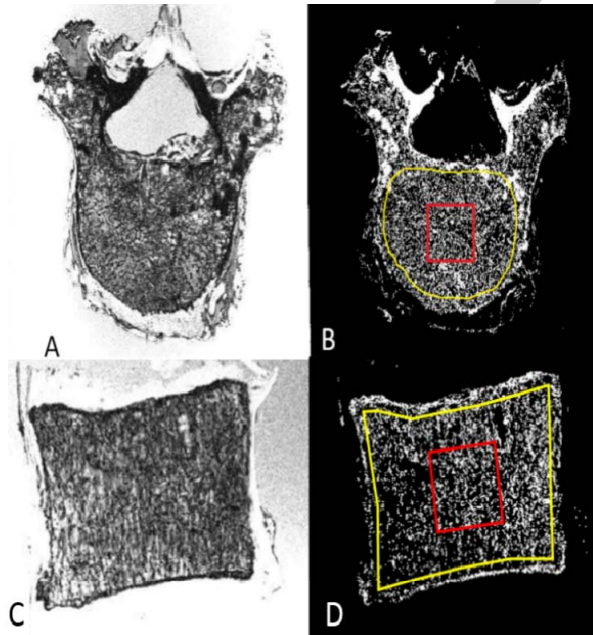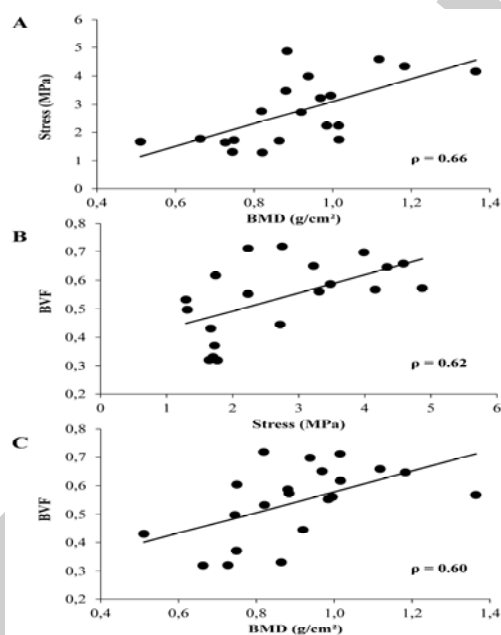
Figure 2: Correlation of bone microarchitecture parameters measured in the whole vertebra and in the cropped volume. A: Bone volume fraction (BVF). B: Trabecular thickness (Tb.Th). C: Trabecular spacing (Th.Sp)
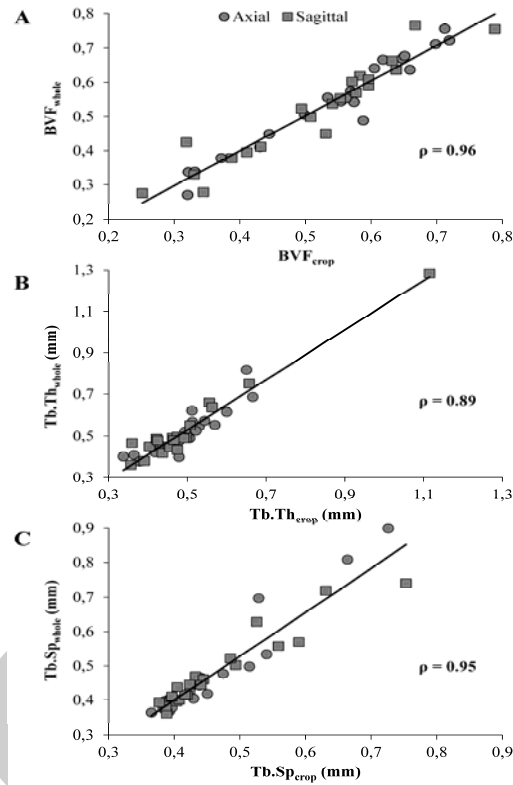
Figure 3: A: Correlation between bone volume fraction (BVF) and Trabecular thickness (Tb.Th) in the axial plane. B: Correlation between BVF and Trabecular spacing (Th.Sp) in the axial plane.
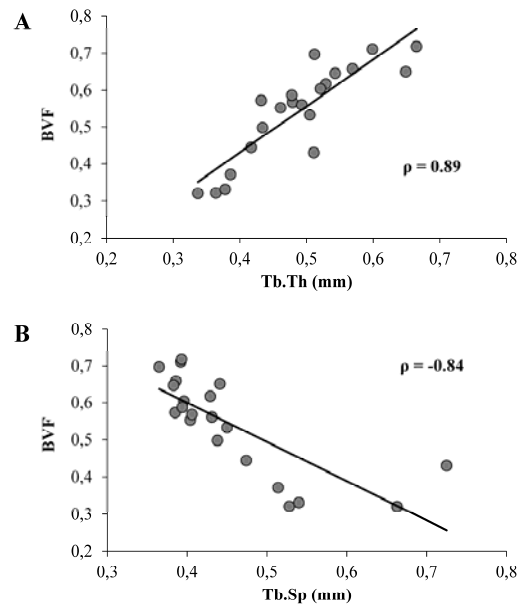
Figure 4: A: Correlation between bone mineral density (BMD) and bone volume fraction (BVF) in the axial plane. B: Correlation between BVF in the axial plane and failure stress. C: Correlation between BVF in the axial plane and BMD.

Tables

Correlation between vertebral microarchitecture parameters and bone mineral density

	BVF Ax	Tb.Th Ax	TbSp Ax	BVF Sag	Tb.Th Sag	Tb.Sp Sag
BVF Ax						
Tb.Th Ax	0.887 *0.0001*					
TbSp Ax	-0.571 *0.007*	-0.306 *0.177*				
BVF Sag	0.797 *0.0001*	0.648 *0.001*	-0.515 *0.017*			
Tb.Th Sag	0.657 *0.001*	0.607 *0.004*	-0.367 *0.010*	0.877 *0.0001*		
Tb.Sp Sag	-0.768 *0.0001*	-0.489 *0.024*	0.665 *0.001*	-0.837 *0.0001*	-0.592 *0.005*	
BMD	0.596 *0.004*	0.474 *0.030*	-0.361 *0.108*	0.461 *0.036*	0.372 *0.097*	-0.511 *0.018*

Table 1: Correlation coefficients (Spearman test, *p value*) between bone volume fraction (BVF) and other microarchitecture parameters (Trabecular thickness (Tb.Th) and trabecular spacing (Tb.Sp)) measured in the axial (Ax) and sagittal (Sag) plane and obtained at UHF-MRI, and bone mineral density (BMD) measured by DXA.

Correlation between biomechanical compression test and vertebral microarchitecture parameters

	Load (N)	Stress (Mpa)
BVF Ax ρ	0.516	0.626
	0.020	*0.003*
Sag ρ	0.326	0.501
	0.160	*0.024*
Tb.Th Ax ρ	0.355	0.359
	0.125	*0.120*
Sag ρ	0.370	0.496
	0.108	*0.026*
Tb.Sp Ax ρ	-0.538	-0.671
	0.014	*0.001*
Sag ρ	-0.460	-0.620
	0.041	*0.004*

Table 2: Correlation Spearman ρ coefficients between failure load and stress, and vertebral bone volume fraction (BVF), trabecular thickness (Tb.Th) and trabecular spacing (Tb.Sp) measured in axial and sagittal plane with *p* values in italic.